An Ab Initio Quantum Chemical and Kinetic Study of the NNH + O Reaction Potential Energy Surface: How Important Is This Route to NO in Combustion?

Naomi L. Haworth, John C. Mackie,* and George B. Bacskay

School of Chemistry, University of Sydney, Sydney, NSW 2006, Australia

Received: February 18, 2003; In Final Form: June 4, 2003

A detailed study of the NNH + O reaction potential energy surface using coupled cluster [CCSD(T)] and density functional (B3LYP) methods is reported. Three N_2OH adducts have been located on this surface: *cis*- and *trans*-ONNH and ONHN. The product channels to NO + NH, N_2O + H, N_2 + OH, and HNO + N have been characterized via the computation of minimum energy paths and of the appropriate transition states. Rate coefficients for the reaction of NNH + O to each of these reaction channels have been computed using RRKM techniques. As the reaction flux passing to these channels in combustion systems is very sensitive to the stability of NNH, the heats of formation of this species and of the transition state leading to its formation (NN−H) were also computed via complete basis estimates of the CCSD(T) energetics based on extrapolation of aug−cc−pV*x*Z results with $x = 5, 6$ obtaining a value of $\Delta_f H^\circ_{298} = 60.6 \pm 0.5$ kcal mol^{-1}. Additionally, a value of $k_4 = 7.80 \times 10^{10} T^{0.642} \exp(1380 \text{ cal mol}^{-1}/RT)$ cm^3 mol^{-1} s^{-1} for the rate coefficient of the reaction NNH + O → NO + NH (4) between 1000 and 2600 K was obtained. This is approximately a factor of 4 less than the previous estimate of k_4 (Bozzelli, J. W.; Dean, A. M., *Int. J. Chem. Kinet.* **1995**, *27*, 1097). The new NNH rate data and thermochemistry are used to predict the level of NO produced in lean combustion in a completely stirred flow reactor. The overall conclusion arrived at on the basis of this work is that, in most combustion systems, the NNH + O pathway represents a very minor route to NO.

Introduction

The presence of nitric oxide in the atmosphere is largely the consequence of combustion processes. As a result, many governments have recently placed stringent limits on the levels of emission of NO from combustion facilities. It is important in the development of new combustion technology that accurate chemical kinetic models of the combustion process be developed to predict the concentrations of NO produced.

Nitric oxide is produced in combustion via four main pathways.[1] The first of these is the well-known Zel'dovich or thermal route, initiated by the reaction

$$N_2 + O \rightleftharpoons N + NO \quad (1)$$

The prompt-NO route is initiated by

$$CH + N_2 \rightleftharpoons HCN + N \quad (2)$$

A third route involves the formation of the intermediate, N_2O, and for fuels containing fuel-bound nitrogen, there is a fuel−NO route.

Recently, Bozzelli and Dean[2] have discovered an additional pathway involving the intermediate NNH radical, formed by the reaction of H with molecular nitrogen,

$$N_2 + H \rightleftharpoons NNH \quad (3)$$

The subsequent reaction of NNH with atomic oxygen then yields the products NO and NH

$$NNH + O \rightarrow NO + NH \quad (4)$$

Using the QRRK technique, Bozzelli and Dean[2] estimated the rate coefficient for this reaction to be $k_4 = 7 \times 10^{13}$ cm^3 mol^{-1} s^{-1} at 2000 K. This reaction and its rate coefficient have been subsequently incorporated into detailed chemical kinetic reaction models such as GRIMech 2.11[3] and its successor, GRIMech 3.0,[4] developed to predict species profiles in the combustion of C_1 and C_2 hydrocarbons.

There have been no direct experimental studies of the reactions of NNH + O → products. In a study of NO profiles in laminar premixed flames of $H_2/O_2/N_2$, however, Hayhurst and Hutchinson[5] observed enhanced production rates of NO in the burnt gases that could not be explained on the basis of the Zel'dovich mechanism alone. They attributed their faster observed rates to the operation of the NNH + O pathway, and from a steady-state analysis of their experimental NO profiles, arrived at a value of $k_4 K_{P,3} = 1.4 \times 10^9 \exp(-2760/T)$ cm^3 mol^{-1} s^{-1} over the temperature range of 1800−2500 K, where k_4 is the rate coefficient of reaction 4 and $K_{P,3}$ is the equilibrium constant of reaction 3. From estimates of the NNH thermochemistry, they evaluated the equilibrium constant and arrived at a value of $k_4 = 1 \times 10^{14}$ cm^3 mol^{-1} s^{-1}, constant within a factor of 2.5, over the temperature range of 1800−2500 K. This result is comparable with the rate coefficient originally estimated by Bozzelli and Dean.[2]

In a study of low-temperature premixed hydrogen-air flames at 38 and 78 Torr pressures, Harrington et al.[6] detected NO levels of about 0.3 ppm and claimed that this level of NO was consistent with the Bozzelli and Dean mechanism.[2] Observation of a fast rate of reaction between NO and NH in shock tubes (where reaction products were not detected) at temperatures between 2220 and 3350 K has also been attributed to the onset of an O + NNH product channel.[7]

* Corresponding Author. E-mail: j.mackie@chem.usyd.edu.au.

10.1021/jp034421p CCC: $25.00
Published on Web 08/12/2003

More recently, experimental and modeling studies of NO profiles in premixed flames[8] and in completely stirred reactors[9] have concluded, however, that in circumstances where the NNH + O route is likely to be important (i.e., where the thermal and prompt NO routes are unimportant), models which employ the above rate coefficient for reaction 4 lead to over-prediction of NO production.

The current study is therefore motivated to make a detailed investigation of the NNH + O reaction potential energy surface using current techniques of computational quantum chemistry. Such a study will allow the calculation of reliable thermochemical and kinetic data that can subsequently be applied to the modeling of combustion reactions in the presence of nitrogen.

Following Bozzelli and Dean, we have also included

$$NNH + O \rightarrow N_2O + H \tag{5}$$

and

$$NNH + O \rightarrow N_2 + OH \tag{6}$$

in our system of reactions (in addition to reactions 3 and 4) as potentially competing channels to reaction 4.

Reactions 4−6 are expected to take place via a common ONNH intermediate, which decomposes to yield NO + NH, N_2O + H, or N_2 + OH. While no studies of the O + NNH association have previously been reported, the three decomposition reactions have been extensively investigated in the chemical literature over the past 18 years.[10−19] It has been found that ONNH, a planar molecule, is stable in both cis and trans forms. Although the latter is generally predicted to be the more stable,[12−15] it has been concluded that decomposition to N_2O + H and N_2 + OH actually occurs via the cis isomer.[14,15]

Several other reactions are also considered in this work, in particular

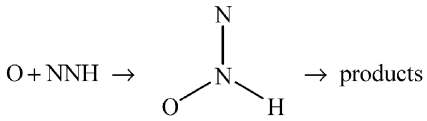

(7)

where the intermediate, ONHN, is an isomer of ONNH that can yield HNO + N, N_2O + H, and N_2 + OH as decomposition products. The isomerization reactions between *cis*- and *trans*-ONNH and between *trans*-ONNH and ONHN are alternative channels, which have also been studied, along with the direct abstraction reaction

$$O + NNH \rightarrow N_2 + OH \tag{8}$$

The stability of the NNH intermediate plays a crucial role in determining the relative importance of channels 4, 5, and 6 in the chemistry of nitrogen in flames, in particular, the reaction flux that passes through channel 4 to generate NO. High level quantum chemical calculations by Walch and Partridge[20] and by Gu et al.[21] have predicted the exothermicity of reaction 3 to be between 3.8 and 4.3 kcal mol^{-1}, with a barrier height of 10.0−11.3 kcal mol^{-1}. As modeling studies are extremely sensitive to the stability of NNH, in the present work, we have also undertaken the computation of the heats of formation of both NNH and the transition state leading to its formation (NN−H) at the highest currently achievable level of theory available to us, namely complete basis estimates of the CCSD(T) (coupled cluster theory with single, double, and perturbative triple excitations) energetics based on extrapolation of aug−cc−pV*x*Z results with $x = 5, 6$.

This work therefore involves an extensive investigation of the N_2OH potential-energy surface using high level quantum chemical methods followed by the computation of the rate parameters for all O + NNH → products channels. We also investigate, on the same potential energy surface, the reaction NO + NH → all product channels and compare our results with existing experimental values of these reactions. Finally, in conjunction with the data set of the GRIMech 3.0 model, we use our revised thermochemistry and rate data to model the lean combustion of CO/H_2/air and CH_4/air in completely stirred reactors as well as low-pressure premixed H_2/air flames under the experimental conditions of Harrington et al.[6]

Theory and Computational Methods

Quantum Chemical Calculations of Thermochemistry. Heats of formation and other thermochemical data were computed via two different approaches: the Gaussian-3X (G3X) method of Curtiss et al.[22] and a CCSD(T)/CBS type scheme, utilizing coupled cluster theory with single, double, and (perturbative) triple excitations (CCSD(T))[23,24] in conjunction with the correlation consistent basis sets,[25−27] aug−cc−pVQZ and aug−cc−pV5Z, and extrapolation to the hypothetical complete basis set (CBS) limit.

In both schemes, molecular geometries and vibrational frequencies for equilibrium structures and transition states were determined by density functional theory (DFT), using the B3LYP hybrid density functional[28−30] with the 6-31G(2*df*,*p*) basis set (frequencies scaled by 0.9854). Single point energy calculations were then performed at these geometries as required for the two different methodologies, namely G3X and CCSD(T)/CBS. Open shell systems were treated by unrestricted calculations in the DFT geometry optimizations (UB3LYP) and the subsequent implementation of G3X but by restricted, RCCSD(T), methods in the CCSD(T)/CBS computations.

In the case of the CCSD(T)/CBS{Q,5} scheme, the single point energies were extrapolated to the complete basis limit using the x^{-3} extrapolation[31]

$$E(x) = A + Bx^{-3} \tag{9}$$

where $x = 4, 5$. In the case of a few species (e.g., NNH) more extensive calculations were performed where the sequence of basis sets include aug−cc−pV6Z, namely $x = 6$. Core−core and core−valence (CV) correlation corrections were evaluated at the CCSD(T)/aug−cc−pCVQZ level of theory. Scalar relativistic effects (Darwin and mass-velocity terms[32,33]) were determined by complete active space SCF (CASSCF)[34,35] theory using cc−pVTZ basis sets. Spin−orbit corrections were also included for atomic species.[36]

As several important reactions, including the formation of ONNH and its decomposition to NO + NH, are barrierless, variational transition state theory (VTST)[37−39] was utilized to locate and characterize the transition states at a range of temperatures between 1000 and 2500 K. As in previous work of ours,[40] density functional theory (B3LYP/6-31G(2*df*,*p*)) was used to map the minimum energy path (MEP) along the potential energy surface (PES) as a function of the reaction coordinate. The latter was approximated as the critical bond-forming or bond-breaking distance; thus, this critical bond distance was systematically varied while all other geometric parameters were allowed to relax. At each such point along the reaction coordinate, the rate coefficient was calculated by the application

of the canonical transition state formula[41] at the given temperature, thus allowing the geometry that yielded the minimum rate to be identified as the variational transition state.

Among the reactions studied in this work, there are several hydrogen transfer reactions (e.g., ONNH → N_2 + OH) as well as two reactions that involve NH bond fissions. Quantum mechanical tunneling might be expected to be of some importance in such reactions at low temperatures. The study of the H + H_2 → H_2 + H exchange reaction by Shavitt[42] provides useful estimates of the tunneling correction to the rate coefficients of this reaction, which could be used as a guide for other hydrogen transfer or migration reactions. While in the range of 200−400 K, the tunneling correction factor calculated by Shavitt[42] varies approximately from 5 to 2; at 1000 K, its value was computed to be 1.16 at most. As the temperature range in our studies is 1000−2600 K, we believe that we can safely assume that tunneling, which we neglect in our work, will have negligible effect on our computed rate coefficients in comparison with the errors implicit in the quantum chemical computation of barrier heights.

The Gaussian 98 programs[43] were used to perform all DFT calculations (geometry optimizations and PES scans) as well as the G3X calculations, while MOLPRO[23,44,45] was utilized for all (R)CCSD(T) computations. The CASSCF calculations of scalar relativistic corrections were carried out using DALTON[46] for all molecules and MOLCAS[47] for atomic species. The computations were performed on DEC alpha 600/5/333 and COMPAQ XP100/500 workstations of the Theoretical Chemistry group at the University of Sydney and on the COMPAQ AlphaServer SC system of the Australian Partnership for Advanced Computing National Facility at the National Supercomputing Centre, ANU, Canberra.

Derivation of Rate Coefficients for Individual Reaction Channels. As discussed above, addition of O to NNH produces three intermediates via chemical activation. These intermediates, which correspond to local minima on the potential energy surface, are *trans*-ONNH, *cis*-ONNH, and ONHN. Further reaction leads to four product channels, namely, to NO + NH, N_2O + H, N_2 + OH, and HNO + N. All but the last of these are exothermic processes. To derive rate coefficients for the overall reaction to the four product channels, we have separately considered the three reaction surfaces for

$$\mathrm{NNH + O} \rightleftharpoons \textit{trans}\text{-ONNH} \rightarrow \text{products} \qquad (10)$$

$$\mathrm{NNH + O} \rightleftharpoons \textit{cis}\text{ - ONNH} \rightarrow \text{products} \qquad (11)$$

and

$$\mathrm{NNH + O} \rightleftharpoons \mathrm{ONHN} \rightarrow \text{products} \qquad (12)$$

We then assume that the vibrationally excited adduct (*trans*-ONNH, *cis*-ONNH or ONHN), is formed from NNH and O at an energy, E, and will undergo the reverse reaction at an energy-specific rate coefficient $k(E)$. The limiting high-pressure rate coefficient for this reverse (dissociation) reaction, $k_{\mathrm{uni},\infty}$, is given by

$$k_{\mathrm{uni},\infty} = \frac{1}{q(T)} \int_{E_0}^{\infty} k(E)\rho(E) \exp(-E/k_B T)\mathrm{d}E \qquad (13)$$

where $q(T)$ is the internal partition function of the adduct calculated at the translational temperature, T, $\rho(E)$ is the density of states, and k_B is Boltzmann's constant. The lower limit for integration is the critical energy of reaction, E_0. The recombination rate coefficient in the high-pressure limit, $k_{\mathrm{rec},\infty}$, is obtained from $k_{\mathrm{uni},\infty}$ by detailed balance using the equilibrium constant $K_c(T)$ as given by

$$k_{\mathrm{rec},\infty} = \frac{k_{\mathrm{uni},\infty}}{K_c(T)} \qquad (14)$$

Once each of the three adducts is formed, all possible isomerizations between the resulting adduct wells are allowed to take place. The overall pressure-dependent rate coefficient via each adduct to each of the product channels is obtained from

$$k_{\mathrm{overall}} = f_{\mathrm{products}} \times k_{\mathrm{rec},\infty} \qquad (15)$$

where f_{products} is the fraction of reaction flux to each product channel. We have carried out an RRKM analysis using the MultiWell suite of programs developed by Barker[48] to solve the internal master equation with densities of states calculated by an exact count method. Collisional energy transfer parameters were taken from the work of Barker.[49] These values are γ = 0.7, $\alpha(E) = 43.5 + 0.0042E$ cm^{-1} for the collision step-size distribution function $f_d(E,E') = \exp\{-[((E' - E)/\alpha(E'))]^{\gamma}\}$, $E' > E$. (See ref 49) Lennard-Jones parameters have been taken from the Chemkin Collection.[50] For an N_2 collider, σ = 3.62 Å, ϵ/k_B = 97.5 K; for the N_2OH adducts (on the basis of the analogous parameters of N_2O, NCO, NCN, and NCNO[50]) we have chosen σ = 3.83 Å and ϵ/k_B = 232 K. As all three adducts lead to the four reaction channels (but with different values of f_{products}), the final overall rate coefficients for NNH + O → products were obtained by summing the contributions from the three surfaces.

In a similar manner, we have used the same reaction potential energy surfaces to calculate rate coefficients to individual product channels for all products from the reaction between NO + NH. Initially, recombination leads either to *trans*- or *cis*-ONNH, followed by isomerization to the three ONNH adducts and subsequent product formation.

Results and Discussion

Quantum Chemistry. All potential stationary points on the O + NNH PES were investigated using B3LYP/6-31G(2*df*,*p*) on both the A′ and A″ surfaces. The A′ species were found to be consistently lower in energy (as found by other workers), so in general, only results for this surface are presented.

The electronic energies of the stationary points on the PES as calculated at the (valence correlated) CCSD(T)/aug−cc−pVQZ and CCSD(T)/aug−cc−pV5Z levels of theory, along with the extrapolated results, are presented in Table 1. The corresponding geometries, rotational constants and vibrational frequencies are summarized in Tables S1 and S2 of the Supporting Information. Table 1 also provides details of CCSD(T)/aug−cc−pCVQZ core valence correlation corrections, scalar relativistic corrections, and the zero point energies for each molecule, and thus, the total CCSD(T)/CBS energy at 0K together with the corresponding G3X result. The thermal corrections between 0 and 298K for each molecule are also reported here. Unfortunately, it was not possible to perform such CCSD(T)/CBS calculation on the cis to trans transition state of ONNH, as the lack of symmetry in this molecule made the aug−cc−pV5Z, as well as the aug−cc−pCVQZ RCCSD(T) calculations too large.

Table 2, in turn, contains the atomization energies for each species, as calculated using both the CCSD(T)/CBS and G3X approaches, as well as the resulting heats of formation at 0 and 298 K, along with literature values for the latter where available.

TABLE 1: Total CCSD(T) and G3X Energies, Core-Valence (CV) Correlation Corrections, Scalar Relativistic Corrections (in E_h) Along With Zero Point Energies and Thermal Corrections to Enthalpies (in kcal mol^{-1})

		valence correlated energy			CV corr	ΔE_{rel}	ZPE	total energy[b]		$H^0_{298} - H^0_0$
		CCSD(T) aug−cc−pVQZ	CCSD(T) aug−cc−pV5Z	CCSD(T) CBS{Q,5}[a]	CCSD(T) aug−cc−pCVQZ	CASSCF cc−pVTZ	B3LYP 6−31G(2*df*,*p*)	CCSD(T) CBS{Q,5}	G3X	B3LYP 6-31G(2*df*,*p*)
N		−54.52506	−54.52780	−54.53068	−0.05613	−0.02921		−54.61601	−54.56490	1.04
O		−74.99493	−75.00041	−75.00615	−0.05907	−0.05237		−75.11795	−75.03224	1.04
H		−0.49995	−0.49999	−0.50004	0.00000	0.00000		−0.50004	−0.50097	1.01
N_2	$^1\Sigma_g$	−109.40724	−109.41551	−109.42418	−0.11344	−0.05818	3.42	−109.59034	−109.48808	2.07
NH	$^3\Sigma$	−55.15574	−55.15913	−55.16269	−0.05628	−0.02906	4.57	−55.24075	−55.19350	2.07
NO	$^2\Pi$	−129.75792	−129.76818	−129.77893	−0.11585	−0.08085	2.80	−129.97117	−129.83624	2.07
OH	$^2\Pi$	−75.66426	−75.67038	−75.67680	−0.05929	−0.05187	5.21	−75.77967	−75.69607	2.07
NNH	$^2A'$	−109.90091	−109.90907	−109.91763	−0.11344	−0.05790	8.18	−110.07595	−109.97501	2.39
NNO	$^1\Sigma$	−184.46683	−184.48141	−184.49671	−0.17313	−0.10956	6.98	−184.76828	−184.58323	2.27
HNO	$^1A'$	−130.34240	−130.35288	−130.36388	−0.11587	−0.08067	8.54	−130.54681	−130.41227	2.37
trans-ONNH	$^2A'$	−185.00994	−185.02643	−185.04373	−0.17290	−0.10949	13.04	−185.30534	−185.11715	2.52
cis-ONNH	$^2A'$	−185.00041	−185.01644	−185.03325	−0.17297	−0.10948	12.56	−185.29569	−185.10725	2.56
ONHN	$^2A'$	−184.97089	−184.98820	−185.00636	−0.17270	−0.10952	12.52	−185.26863	−185.07844	2.53
NN−H	$^2A'$	−109.88513	−109.89336	−109.90200	−0.11332	−0.05813	4.05	−110.06699	−109.96623	2.46
ONN−H	$^2A'$	−184.95143	−184.96843	−184.98626	−0.17301	−0.10955	7.38	−185.25707	−185.06898	2.76
ON_2-H	$^2A'$	−184.92953	−184.94647	−184.96424	−0.17276	−0.10957	7.77	−185.23418	−185.04605	2.57
NNOHsq	$^2A'$	−184.94179	−184.95694	−184.97283	−0.17210	−0.10985	8.91	−185.24059	−185.05381	2.50
NNOHtr	$^2A'$	−184.92091	−184.93646	−184.95278	−0.17257	−0.10976	8.20	−185.22205	−185.03713	2.71
ONNH c−t TS	$^2A'$								−185.08082	
ONHN−ONNHt	$^2A'$	−184.91787	−184.93264	−184.94813	−0.17260	−0.10956	9.02	−185.21592	−185.03186	2.63

[a] Extrapolated CCSD(T) energy to CBS ($x = \infty$)limit using $x = 4,5$ data. [b] Including CV, ΔE_{rel} and ZPE corrections in CCSD(T)/CBS energies.

TABLE 2: CCSD(T)/CBS{Q,5} and G3X Atomization Energies (Along With CV Correlation and Scalar Relativistic Contributions to CBS) and Heats of Formation (at 0 and 298 K) of Reactants, Products, Intermediates, and First Order Saddle Points on the N_2OH Surface (in kcal mol^{-1})

	atomization energy[a]				$\Delta_f H^0_0$		$\Delta_f H^0_{298}$		
	CV corr	ΔE_{rel}	CCSD(T)[b]/CBS	G3X	CCSD(T)[b]/CBS	G3X	CCSD(T)[b]/CBS	G3X	experiment
N_2	0.74	−0.15	224.9	224.8	0.2	0.2	0.2	0.2	0.00
NH	0.09	−0.09	78.3	80.1	85.9	84.1	85.9	84.1	85.32 ± 0.02[c]
NO	0.41	−0.46	148.9	150.0	22.7	21.5	22.7	21.5	21.82 ± 0.04[d]
OH	0.14	−0.31	101.5	102.2	9.2	8.4	9.2	8.5	8.83 ± 0.09[e]
NNH	0.74	−0.33	215.8	216.0	60.9	60.7	60.2	60.0	
NNO	1.13	−0.77	262.5	264.3	21.6	19.8	20.7	18.9	19.6 ± 0.1[f]
HNO	0.42	−0.57	196.3	197.1	26.9	26.0	26.2	25.3	$25.6^{+0.6}_{-0.1}$[g]
trans-ONNH	0.99	−0.82	285.7	285.0	50.0	50.7	48.4	49.1	
cis-ONNH	1.03	−0.82	279.7	278.8	56.0	56.9	54.5	55.4	
ONHN	0.86	−0.80	262.7	260.7	73.0	75.0	71.4	73.4	
NN−H	0.67	−0.18	210.2	210.5	66.5	66.2	65.9	65.6	
ONN−H	1.05	−0.78	255.4	254.8	80.3	80.9	78.9	79.6	
ON_2−H	0.90	−0.77	241.1	240.4	94.6	95.3	93.1	93.8	
NNOHsq	0.48	−0.59	245.1	245.2	90.6	90.5	89.0	88.8	
NNOHtr	0.78	−0.65	233.5	234.8	102.2	100.9	100.8	99.5	
ONNH c−t TS				262.2		73.5		71.9	
ONHN−ONNHt	0.80	−0.77	229.6	231.5	106.1	104.2	104.6	102.7	

[a] Including zero-point corrections. [b] Including CV correlation and scalar relativistic corrections. [c] Ref 51. [d] Ref 52. [e] Ref 53. [f] Ref 52. [g] Ref 54.

Core-valence correlation and relativistic contributions to the atomization energies are also included in this table. Examination of the latter reveals that both effects are relatively small in magnitude and that their respective contributions cancel out to a large extent, resulting in a net contribution of ~0.5 kcal mol^{-1} or less.

According to Curtiss et al.,[22] the heats of formation obtained from the G3X method are expected to have a *mean* absolute deviation of 1.0 kcal mol^{-1} from experiment. The CCSD(T)/CBS results are expected to have a higher degree of accuracy; our conservative estimate for the maximum uncertainty in *any* of the heats of formation computed via CCSD(T)/CBS in this work is ± 1.0 kcal mol^{-1}. Comparison of the CCSD(T)/CBS and G3X heats of formation indicates the two sets of results agree with each other and with the available experimental data within their respective error margins.

In light of the sensitivity of the kinetic models to the stability of NNH, as noted above, a more extensive investigation was carried out for NNH, N_2, and the transition state, NN−H. The geometries and harmonic frequencies were redetermined at the CCSD(T)/aug−cc−pVQZ level of theory using numerical differentiation to obtain the appropriate force constants. The CCSD(T) valence correlated energies were calculated at the revised geometries using the aug−cc−pV5Z and aug−cc−pV6Z basis sets[55,56] and extrapolated as before. CCSD(T)/aug−cc−pCVQZ CV corrections, CASSCF/cc−pVTZ scalar relativistic corrections and atomic spin−orbit corrections were again applied. To account, at least in part, for the effects of anharmonicity in the calculation of the zero-point energies and thermal corrections, the NNH bending frequencies were scaled by a factor of 0.97, the NN stretching frequencies by 0.988, and the NH stretching frequencies by 0.95. (These scaling factors were chosen by comparison of experimental harmonic and anharmonic frequencies of N_2, NH_3, and H_2O.) The results of these high level calculations are summarized in Table 3. As can be seen by comparison with the results in Table 2, the application of a substantially higher level of theoretical treatment leaves the heats of formation for N_2 and NNH largely unchanged; it

TABLE 3: Summary of the Energetic Contributions to the CCSD(T)/CBS{5,6} Extrapolated Atomization Energies (*AE*) and Heats of Formation for N_2, NNH, and the NN−H Transition State (in E_h Unless Otherwise Noted)

	N	H	N_2	NNH	NN−H
CCSD(T)/aug−cc−pV5Z	−54.52780	−0.49999	−109.41550	−109.90913	−109.89164
CCSD(T)/aug−cc−pV6Z	−54.52865	−0.50000	−109.41838	−109.91167	−109.89596
CCSD(T)/CBS{5,6}	−54.52982	−0.50001	−109.42233	−109.91517	−109.90200
CCSD(T)/aug−cc−pCVQZ (core + valence)	−54.58205		−109.52248	−110.01611	−109.99847
CCSD(T)/aug−cc−pCVQZ (valence only)	−54.52592		−109.40906	−109.90267	−109.88515
CV correction	−0.05613		−0.11342	−0.11343	−0.11332
ΔE_{rel}	−0.02921		−0.05818	−0.05790	−0.05811
ZPE			0.00526	0.01287	0.00644
CCSD(T)/CBS {5,6}[a]	−54.61516	−0.50001	−109.58867	−110.07363	−110.06698
CCSD(T)/CBS {5,6} *AE*[a]/kcal mol^{-1}			224.87	215.43	211.26
CCSD(T)/CBS {5,6} $\Delta_f H_0^0$[a]/kcal mol^{-1}			0.19	61.26	65.43
$H_{298}^0 - H_0^0$/kcal mol^{-1}	1.04	1.01	2.07	2.39	2.44
CCSD(T)/CBS {5,6} $\Delta_f H_{298}^0$[a]/kcal mol^{-1}			0.18	60.56	64.78

[a] Including CV, ΔE_{rel}, and ZPE corrections.

TABLE 4: Energies of NNH and N_2OH Species Relative to N_2 + H and NO + NH, Respectively, Computed at Different Levels of Theory[a] (in kcal mol^{-1})

	CCSD(T) CBS {Q,5}	CCSD(T) CBS {5,6}	G3X	G2[b]	MR−CI[c]	CCSD(T)/ aug-cc-pVQZ[d]	MR−CI + Dav.[e]
NNH	9.1	9.4	8.8			8.6 ± 0.5	9.1
NN−H	14.7	13.6	14.3			14.4 ± 1.0	16.3
trans-ONNH	−58.6		−54.9	−56.0	−51.5		
cis-ONNH	−52.6		−48.6	−48.9	−46.2		
ONHN	−35.6		−30.6				
O + NNH	11.3		14.1				
NNO + H	−35.4		−34.2	−34.5	−31.7		
N_2 + OH	−99.2		−96.9	−96.9			
ONNH c−t TS			−32.1	−30.8			
ONN−H	−28.3		−24.6	−25.3	−21.4		
ON_2−H	−14.0		−10.2				
NNOHsq	−18.0		−15.1	−17.9	−15.4		
NNOHtr	−6.4		−4.6				
ONHN−ONNHt	−2.5		−1.3				

[a] Including zero-point corrections. [b] Ref 15. [c] Ref 14. [d] Ref 21 + B3LYP/6-31G(2*df*,*p*) zero point energy. [e] MR−CI values including Davidson's correction from ref 20 + B3LYP/6-31G(2*df*,*p*) zero point energy.

does, however, reduce the barrier for the dissociation of NNH by ∼1 kcal mol^{-1}.

Comparison of the CCSD(T)/aug−cc−pV5Z energies at the revised CCSD(T) geometries (in Table 3) with those at B3LYP geometries (in Table 1) demonstrate that for N_2 and NNH the small geometric changes (less than 0.01 Å in bond lengths and 0.6° in the NNH bond angle) have a negligible effect on the energies. For the NN−H transition state, however, the energy has been lowered by ∼1 kcal mol^{-1}; this is accompanied by a decrease of 0.12 Å in the N−H bond length. The zero-point energies are effectively unchanged (differences of ∼ 0.1 kcal mol^{-1} or less). For N, N_2, and NNH, the CCSD(T)/CBS{5,6} energies are 0.54, 1.16, and 1.54 kcal mol^{-1} higher than the corresponding {Q,5} results. Thus the effects of the extra degree of theoretical complexity implicit in the aug−cc−pV6Z calculations largely cancel in the atomization energy computations of N_2, while the value for NNH is reduced by ∼ 0.4 kcal mol^{-1}. Interestingly, for the NN−H transition state, the combined effects of geometry changes and larger basis set have resulted in a CCSD(T)/CBS{5,6} energy that is essentially the same as that obtained via CCSD(T)/CBS{Q,5}. The net result is therefore a lower atomization energy for NN−H (i.e., the barrier to dissociation is reduced by ∼1 kcal mol^{-1}). These results are in support of our proposed uncertainty of ± 1 kcal mol^{-1} in our CCSD(T)/CBS heats of formation.

In Table 4, the G3X and CCSD(T)/CBS energetics are compared with the earlier theoretical work of Walch and Partridge,[14,20] Gu et al.,[21] and Durant.[15] As these workers reported their results as energies relative to N_2 + H (for NNH and NN−H) and NO + NH for all other species, we also present our results in this form for easy comparison. Note also that the previous calculations on NNH and NN−H by Walch and Partridge[20] and by Gu, Xie and Schaefer[21] reported only electronic energy differences; we have therefore added our B3LYP/6-31G(2*df*,*p*) zero-point energies to their values for consistency. The results of Gu et al.[21] were obtained via CCSD(T)/aug−cc−pVQZ calculations while Walch and Partridge utilized multireference CI (MRCI) (including Davidson's correction) in conjunction with the cc−pV*x*Z, x = D, T, Q, 5 basis sets and extrapolation via the exponential formula

$$E(x) = A + B\exp(-Cx) \tag{16}$$

While there is broad agreement with respect to the stability of NNH, our best estimate of the barrier height for its dissociation is lower than those obtained by either of the other groups. Thus, our results indicate that NNH is significantly less stable to dissociation and has a shorter lifetime than previously predicted.

The energies of the N_2OH species are compared in Table 4 with the G2 values of Durant[15] and the MRCI results of Walch.[14] As may be expected, the G2 and G3X results are, in most cases, in good agreement. The MRCI results of Walch, however, are found to be consistently higher than those obtained by either G2, G3X, or CCSD(T)/CBS. We believe that this discrepancy

is due to size extensivity problems in the MRCI approach, which in this case, did not include Davidson's correction. Such problems are expected to be most serious in the calculation of dissociation energies. Consequently, as noted by Durant,[15] in Walch's calculations, the stabilities of the N_2OH species (as well as of N_2O + H) relative to NO + NH are underestimated by ~3 kcal mol^{-1}; when a correction of this size is applied to the MRCI results, the agreement with the G2 and G3X results is much improved. It is seen, however, that the CCSD(T)/CBS{Q,5} results are generally significantly lower than their G3X counterparts, by up to 3.7 kcal mol^{-1}.

We believe that for the systems studied here, the CCSD(T)/CBS approach, as outlined in this work, represents potentially the highest level of size consistent treatment of electron correlation that is currently available. Consequently, we expect our CCSD(T)/CBS results to be more accurate than those obtained previously.

Potential Energy Surfaces and Reaction Paths. Schematic potential energy diagrams showing the major stationary points on the N_2OH potential energy surface corresponding to the three main reaction channels (Equations (10) to (12)) are shown in Figures 1 to 3. The relative enthalpies (at 298K) shown in these diagrams are CCSD(T)/CBS{Q,5} values, except for ONNH c−t TS where the G3X result has been used. Clearly, the reaction channels producing N_2O + H and N_2 + OH are thermodynamically favored over the formation of NO + NH. On the other hand, the reaction to form N + HNO is calculated to be endothermic by 19.4 kcal mol^{-1} and is thus unlikely to compete with the other more favorable channels.

As several of the reactions on this PES involve barrierless recombinations or dissociations, variational transition state theory was applied to locate and characterize the (temperature dependent) transition states, as described in the Theory and Computational Methods section. Energies, and thus heats of formation, at the CCSD(T)/CBS level of theory were estimated by utilizing the B3LYP/6-31G(2*df*,*p*) estimate of the energy difference between the transition state and the dissociated adducts along with the CCSD(T)/CBS energies for the dissociated species. The resulting heats of formation are listed in Table 5. Geometries, rotational constants and vibrational frequencies for these species are given in Tables S3 and S4 of the Supporting Information.

As noted in the Theory and Computational Methods section, the MEP's for all potential reaction channels were mapped using B3LYP/6-31G(2*df*,*p*). The important features of each surface are discussed here.

NNH ($^2A'$) + *O* (^3P) → *cis- and trans-ONNH* ($^2A'$). Both reactions, as indicated in Figures 1 and 2, are simple barrierless recombinations leading to the *cis*- and *trans*-ONNH adducts. Variational transition states were determined for both reactions, as described in the section on Theory and Methods. In the vicinity of the minima for *cis*- and *trans*-ONNH, the cis−trans interconversion takes place via torsion. The ONNH dihedral angle in the isomerization transition state structure, ONNH c-t TS, was found to be 90.9°.

NNH ($^2A'$) + *O* (^3P) → *ONHN* ($^2A'$). This is also a barrierless recombination reaction, as shown in Figure 3. The ONHN adduct and the variational transition states leading to it are all planar. As O approaches NNH, the initial degeneracy of the $^2A'$ and $^2A''$ states is lifted; the ground states of both ONHN and the O−NHN transition state are $^2A'$.

cis- and trans-ONNH ($^2A'$) → *NO* ($^2\Pi$) + *NH* ($^3\Sigma$). The dissociation of both isomers was found to occur via a common, barrierless, nonplanar surface, as shown in Figures 1 and 2. At N−N separations larger than ~ 1.7 Å, the ^2A states of nonplanar ONNH correlate with the $^2A''$ surfaces of planar cis- and *trans*-ONNH, which are known to be barrierless to the NO + NH recombination. The presence of barriers on the $^2A'$ surface has been established by the MRCI studies of Walch.[14] In effect, we are proposing that the dissociation reaction of ONNH occurs via $^2A' \rightarrow {}^2A''$ surface crossing which can be achieved by the out-of-plane distortion, namely torsion of the molecules. This is reasonable for the sort of systems we are modeling, where the ONNH adducts are generated in highly vibrationally excited states as a result of chemical and/or collisional activation. Surface crossing, via vibronic coupling, predominantly involving torsion, is expected to occur readily. The minimum energy paths for such dissociations therefore access nonplanar geometries once the ground states are $^2A''$. Note, however, that even though there is a common MEP for both cis and trans dissociations, their respective variational transition states differ slightly because of the differences in the ground-state energies and partition functions of the two ONNH isomers.

ONHN ($^2A'$) → *N* (^4S) + *HNO* ($^1A'$). This reaction (Figure 3) is complicated by a change in spin multiplicity from doublet to quartet as the N−N bond breaks. By mapping the minimum energy paths on both the doublet and quartet surfaces as a function of N−N distance, it was found that the intersection occurs at a distance of approximately 1.9 Å. The variational transition states for the dissociation at all temperatures are found to occur on the (barrierless) quartet surface at NN distances of ~2.1 Å. We expect that the intersystem crossing will be substantially faster than the classical dissociation, hence the rate of this reaction was calculated using variational transition state and RRKM theory, utilizing the transition state structures identified on the quartet surface.

cis- and trans-ONNH ($^2A'$) → *N_2O* ($^1\Sigma$) + *H* (^2S). The dissociation of the cis isomer takes place over a barrier of

TABLE 5: G3X and CCSD(T)/CBS{Q,5} Heats of Formation (at 0 and 298 K) of Variational Transition States (in kcal mol^{-1})

		$\Delta_f H_0^0$		$\Delta_f H_{298}^0$	
reaction	temp (K)	G3X	CBS	G3X	CBS
trans-ONNH → O + NNH	1000	116.1	116.3	115.1	115.3
	1500	114.2	114.5	113.1	113.4
	2000	112.1	112.3	110.9	111.1
	2500	109.6	109.8	108.3	108.5
cis-ONNH → O + NNH	1000	116.8	117.1	115.9	116.1
	1500	116.2	116.4	115.2	115.4
	2000	114.9	115.1	113.9	114.1
	2500	112.7	112.9	111.5	111.8
ONHN → O + NNH	1000	117.0	117.2	116.1	116.3
	1500	115.5	115.7	114.5	114.8
	2000	111.4	111.7	110.3	110.5
	2200	107.0	107.2	105.7	105.9
trans-ONNH → NO + NH	1000	99.8	102.9	98.9	102.0
	1500	98.6	101.6	97.6	100.6
	2000	97.1	100.1	96.1	99.1
	2400	96.7	99.7	95.6	98.6
cis-ONNH → NO + NH	1000	99.6	102.6	98.7	101.7
	1500	98.2	101.3	97.3	100.3
	2000	96.7	99.7	95.6	98.6
	2500	96.2	99.2	95.1	98.1
ONHN → N + HNO	1000	135.5	136.4	134.2	135.0
	1500	135.1	135.9	133.7	134.6
	2000	134.5	135.3	133.1	133.9
	2500	134.1	135.0	132.7	133.5
NNH + O → N_2 + OH	1000	117.8	118.0	116.8	117.0
	1500	116.9	117.2	115.8	116.1
	2000	115.7	116.0	114.6	114.8
	2500	115.3	115.5	114.1	114.3

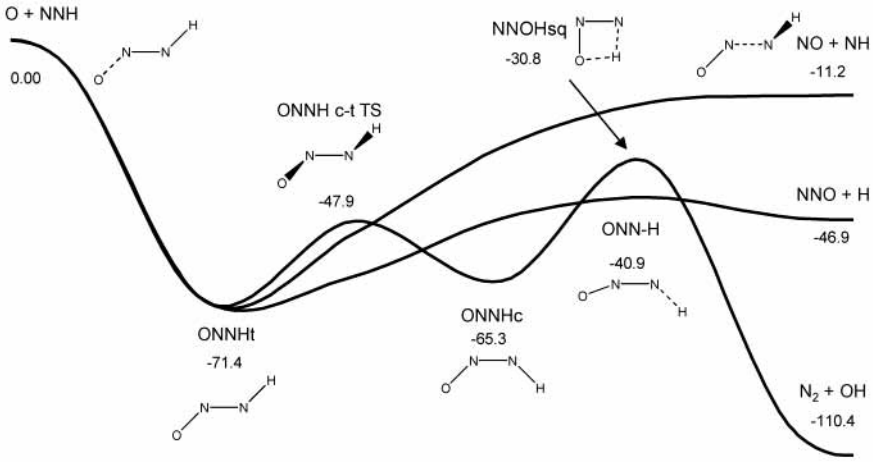

Figure 1. Schematic potential energy surfaces for the reactions of *trans*-ONNH. Relative enthalpies at 298 K (in kcal mol^{-1}) from CCSD(T)/CBS{Q,5} calculations.

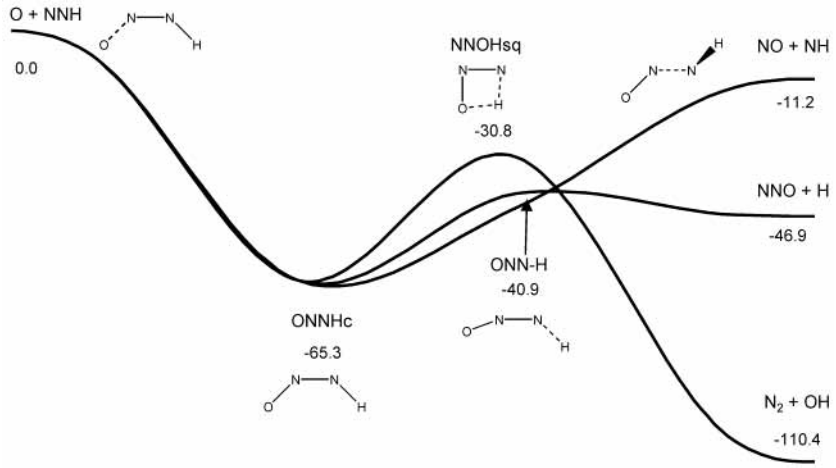

Figure 2. Schematic potential energy surfaces for the reactions of *cis*-ONNH. Relative enthalpies at 298 K (in kcal mol^{-1}) from CCSD(T)/CBS{Q,5} calculations.

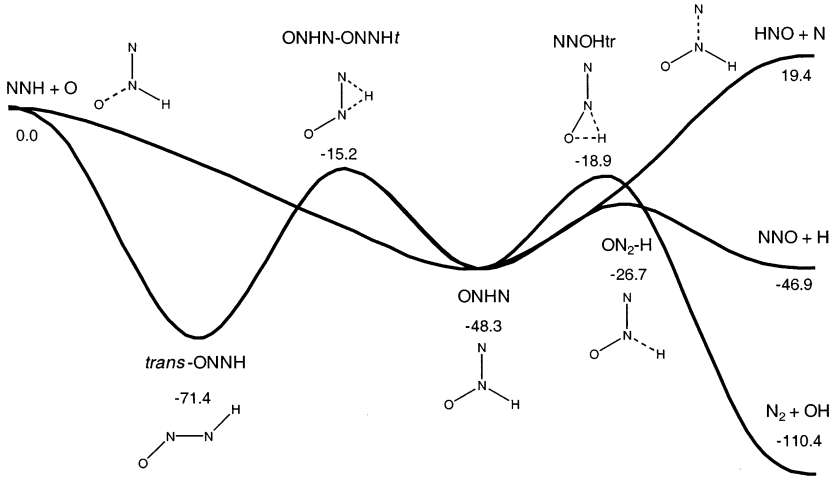

Figure 3. Schematic potential energy surfaces for the reactions of ONHN. Relative enthalpies at 298 K (in kcal mol^{-1}) from CCSD(T)/CBS{Q,5} calculations.

24.4 kcal mol^{-1} (6.1 kcal mol^{-1} above products) as shown in Figure 1. The B3LYP calculations reveal that in this transition state, labeled ONN−H, the ONN moiety is near-linear ($\angle$NNO = 173°) and the N−H separation is 1.66 Å. Attempts to find an analogous transition state on the trans surface were, however, unsuccessful as calculations converged either to the cis transition state or to a second-order saddle point. Mapping the minimum energy path as a function of N−H distance for *trans*-ONNH revealed a monotonic increase in the energy, significantly exceeding the barrier height to ONN−H in the region of R(N−H) $\approx$ 1.50 Å; at this point, however, the NNO angle of 156° is only 24° larger than at equilibrium. Stretching the N−H bond further results in a rapid increase in the NNO angle and collapse onto the cis surface. Further exploration of the potential energy surface revealed that there is a family of low energy ($\sim$5−10 kcal mol^{-1}) trans to cis isomerization

TABLE 6: Rate Coefficients (cm^3 mol^{-1} s^{-1}) for NNH + O → Product Channels Shown via Adducts *cis*-ONNH, *trans*-ONNH and ONHN at 1 atm Pressure

	cis-ONNH				*trans*-ONNH				ONHN			
T/K	NO + NH	N_2O + H	N_2 + OH	HNO + N	NO + NH	N_2O + H	N_2 + OH	HNO + N	NO + NH	N_2O + H	N_2 + OH	HNO + N
1000	6.51×10^{12}	1.64×10^{13}	3.19×10^{12}		9.45×10^{12}	2.17×10^{13}	8.36×10^{11}		3.61×10^{11}	1.94×10^{13}	6.55×10^{12}	
1200	7.23×10^{12}	1.56×10^{13}	3.09×10^{12}		9.35×10^{12}	1.82×10^{13}	6.33×10^{11}		2.52×10^{11}	1.99×10^{13}	6.13×10^{12}	
1400	7.07×10^{12}	1.56×10^{13}	3.18×10^{12}		7.65×10^{12}	1.90×10^{13}	8.13×10^{11}		3.00×10^{11}	1.86×10^{13}	5.88×10^{12}	
1600	7.88×10^{12}	1.52×10^{13}	3.19×10^{12}		7.60×10^{12}	1.66×10^{13}	6.44×10^{11}		5.07×10^{11}	1.70×10^{13}	5.89×10^{12}	3×10^{9}
1800	7.62×10^{12}	1.69×10^{13}	3.55×10^{12}		7.55×10^{12}	1.69×10^{13}	6.07×10^{11}		5.06×10^{11}	2.10×10^{13}	7.22×10^{12}	7×10^{9}
2000	8.16×10^{12}	1.65×10^{13}	3.50×10^{12}		8.09×10^{12}	1.64×10^{13}	5.59×10^{11}		5.40×10^{11}	1.83×10^{13}	6.41×10^{12}	6×10^{9}
2200	8.84×10^{12}	1.60×10^{13}	3.50×10^{12}		7.45×10^{12}	1.35×10^{13}	4.62×10^{11}		5.84×10^{11}	1.60×10^{13}	6.12×10^{12}	12×10^{9}
2400	9.40×10^{12}	1.63×10^{13}	3.58×10^{12}		7.15×10^{12}	1.32×10^{13}	4.89×10^{11}		5.52×10^{11}	1.63×10^{13}	6.10×10^{12}	20×10^{9}
2600	9.77×10^{12}	1.57×10^{13}	3.50×10^{12}		7.05×10^{12}	1.19×10^{13}	4.50×10^{11}	2×10^{9}	5.27×10^{11}	1.43×10^{13}	5.48×10^{12}	16×10^{9}

pathways that occur via the linearization of the NNO moiety, such that the maximum energy is below the energy of ONN−H. In summary, therefore, both *cis*- and *trans*-ONNH dissociate to N_2O + H via a common transition state as shown in Figures 1 and 2, with the understanding that the trans to cis isomerization is part of the overall mechanism.

ONHN ($^2A'$) → *N_2O* ($^1\Sigma$) + *H* (^2S). As shown in Figure 3, this reaction proceeds via a transition state (denoted ON_2−H) with a critical enthalpy of 21.7 kcal mol^{-1} and an exothermicity of 1.4 kcal mol^{-1} at 298 K.

cis-ONNH ($^2A'$) → *N_2* ($^1\Sigma_g$) + *OH* ($^2\Pi$). This reaction (Figure 1) occurs via a cyclic NNOH transition state (designated NNOHsq) followed by dissociation to N_2 + OH. Given the geometry of this transition state, the reaction can only proceed from the cis form of ONNH. The computed reaction barrier is 34.5 kcal mol^{-1} (i.e., ∼10 kcal mol^{-1} higher than that for the N_2O + H channel). However, while ONNH → N_2O + H is endothermic, the ONNH → N_2 + OH reaction is highly exothermic (by 45.1 kcal mol^{-1}).

ONHN ($^2A'$) → *N_2* ($^1\Sigma_g$) + *OH* ($^2\Pi$). This reaction proceeds by a 1,2 hydrogen shift from the central nitrogen to the oxygen, yielding a cyclic transition state, followed by decomposition into N_2 + OH (Figure 3). The transition state has been labeled NNOHtr; it is 29.4 kcal mol^{-1} higher in energy than ONHN and 91.4 kcal mol^{-1} higher than the dissociated products.

NNH ($^2A'$) + *O* (^3P) → *N_2* ($^1\Sigma_g$) + *OH* ($^2\Pi$). This reaction represents the direct abstraction of the hydrogen of NNH by an oxygen atom. Somewhat surprisingly, no barrier was found for this reaction. This is likely to be a consequence of the very weak (breaking) N−H bond and the very strong interaction between the hydrogen and oxygen atoms, which is attractive at all O−H separations.

trans-ONNH ($^2A'$) → *ONHN* ($^2A'$). These two intermediates can interconvert via a 1,2 hydrogen shift, although the barrier is rather high at 53.6 kcal mol^{-1} above *trans*-ONNH and 29.3 kcal mol^{-1} above ONHN (Figure 3). We also considered the possibility that this isomerization could occur via a 1,2 oxygen shift. Although a transition state was found for this process using B3LYP/6-31G(2*df*,*p*), the subsequent RCCSD(T) calculations using this geometry showed large values of the τ_1 diagnostic and are therefore judged to be unreliable. Similarly, the corresponding higher level calculations which make up G3X were also not accepted as reliable due to the presence of significant spin contamination. As the energy of this transition state is ∼ 28 kcal mol^{-1} higher than the analogous H transfer transition state at the B3LYP level of theory, this process was not investigated any further.

Kinetic Parameters. For the three reaction potential energy surfaces (viz., those shown in Figures 1 to 3) chemical activation simulations were carried out over the temperature range of 1000−2600 K and at pressures ranging from 1 to 10000 Torr using the MultiWell code. This temperature range spans the temperatures of relevance in flame studies. For each potential energy surface, there are four barrierless reactions. These are the reverse fission reactions, adduct → NNH + O together with *cis*-ONNH → NO + NH, *trans*-ONNH → NO + NH, and ONHN → HNO + N. For each of these reactions, a variational transition state (VTS) was located at temperatures of 1000 K, 1500 K, 2000 K, and at a higher temperature (2500 K except for *trans*-ON−NH → NO + NH and ONHN→ O + NNH, which were evaluated at 2400 and 2200 K, respectively). The VTS evaluated at 1000 K was used in the MultiWell modeling for temperatures 1000 and 1200 K, the VTS at 1500 K for temperatures 1400 and 1600 K, the VTS at 2000 K for temperatures 1800, 2000, and 2200 K, and the high-temperature VTS for 2400 and 2600 K. Pressure-dependent overall rate coefficients to the four product channels were calculated using eqs 14 and 15.

TABLE 7: Modified Arrhenius Parameters for NNH + O → Products via Adducts *cis*-ONNH, *trans*-ONNH and ONHN [$k = AT^n \exp(-E_a/RT)$]

reactions	A/cm^3 mol^{-1} s^{-1}	n	E_a/cal mol^{-1}
NNH + O → NO + NH	7.80×10^{10}	0.642	−1830.
NNH + O → N_2O + H	2.40×10^{16}	−0.765	1540.
NNH + O → N_2 + OH	2.57×10^{10}	0.702	−2320.
NNH + O → HNO + N	6.2×10^{-7}	4.84	0.
NNH + O → N_2 + OH[a]	3.00×10^{13}	0	0.

[a] Direct abstraction reaction via abstraction transition state.

No stabilization of adducts or intermediates was found at any temperature or pressure in the studied range. Rate coefficients derived for individual reaction channels for a pressure of 1 atm are presented in Table 6. The rate coefficients did not show any significant pressure dependence between 1 and 10000 Torr and were not strongly dependent on temperature. The summed contribution to each channel from the two surfaces can be fitted by a modified Arrhenius expression and these rate coefficients are given in Table 7. From Tables 6 and 7, we see that the major product channel is to N_2O + H, with all three surfaces contributing an approximately equal amount of reaction flux. The main contribution to the N_2 + OH channel is through the intermediate ONHN with a somewhat smaller contribution arising from the *cis*-ONNH. Nearly all flux to NO + NH is through the *cis*- and *trans*- adducts. The endothermic reaction to HNO + N is only a very minor pathway, and nearly all reaction flux is via the ONHN intermediate. A significant additional contribution to the production of N_2 + OH can also arise from the barrierless direct abstraction reaction for NNH + O.

Our branching ratios into the three principal reaction channels are very different from those estimated by Bozzelli and Dean.[2] In their QRRK analysis, they only considered a single ONNH adduct, and they did not consider the ONHN adduct, which we have discovered in the present work. The ONHN well is considerably shallower than that for *cis*- or *trans*-ONNH and

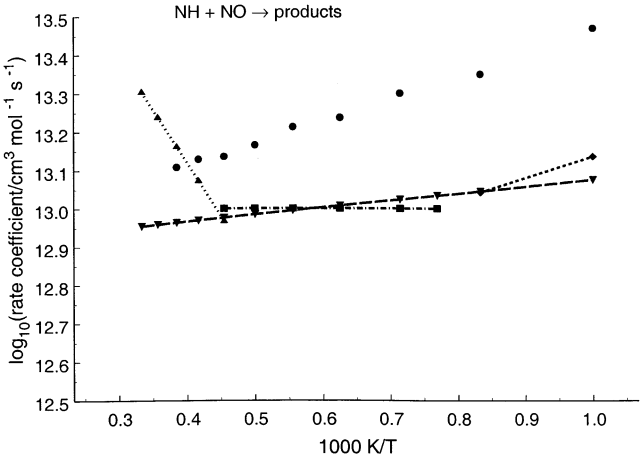

Figure 4. Comparison of rate coefficients for the reaction NO + NH → all product channels computed from the present ab initio reaction potential energy surfaces and experiment. Filled triangles and dotted line = data of Mertens et al.,[7] inverted triangles and dashed line = data of Yokoyama et al.,[58] filled squares and dot−dash line = data of Romming and Wagner,[59] filled diamonds and dashed line = data of Lillich et al.[57] Filled circles = results of present calculations.

TABLE 8: Rate Coefficients (cm^3 mol^{-1} s^{-1}) for Reaction between NO + NH into Individual Product Channels

	product channels			
T/K	O + NNH	N_2O + H	N_2 + OH	all
1000	8.04×10^9	2.76×10^{13}	1.89×10^{12}	2.95×10^{13}
1200	3.31×10^{10}	2.09×10^{13}	1.46×10^{12}	2.24×10^{13}
1400	6.72×10^{10}	1.85×10^{13}	1.40×10^{12}	2.00×10^{13}
1600	1.09×10^{11}	1.58×10^{13}	1.30×10^{12}	1.72×10^{13}
1800	1.18×10^{11}	1.50×10^{13}	1.22×10^{12}	1.63×10^{13}
2000	1.68×10^{11}	1.33×10^{13}	1.16×10^{12}	1.46×10^{13}
2200	2.29×10^{11}	1.23×10^{13}	1.11×10^{12}	1.37×10^{13}
2400	2.79×10^{11}	1.21×10^{13}	1.10×10^{12}	1.34×10^{13}
2600	3.52×10^{11}	1.14×10^{13}	1.07×10^{12}	1.28×10^{13}

significant flux flows through the ONHN adduct both to N_2O + H and to N_2 + OH (but *not* to NO + NH).

For the reaction between NO and NH, simulations were carried out under the same temperature and pressure conditions as those for the O + NNH reaction over the *cis*- and *trans*-ONNH surfaces. (The NO + NH reaction does not initially lead to the ONHN adduct.) All possible isomerizations are allowed and rate coefficients calculated for the exit channels N_2O + H, N_2 + OH, O + NNH, and HNO + N. Again, no stabilization of adducts or intermediates was found at any temperature or pressure in the studied range. Rate coefficients for the reaction NO + NH into individual reaction channels are presented in Table 8.

Comparison with Experiment. Although there have been no experimental measurements of the rate coefficient of reaction 4, the reaction NO + NH → all products has been extensively studied in the last 12 years. However, there is a paucity of rate data for reactions into individual product channels. In Figure 4 we present a compilation of experimental data for the reaction NO + NH → all products, together with our rate data obtained from the ab initio reaction potential energy surfaces. As can be seen from this Figure, there is good agreement among the various experimental measurements. Our calculated rate coefficient of approximately 1×10^{13} cm^3 mol^{-1} s^{-1} between about 2000 and 3000 K also agrees well with experiment. However, the steep rise in the rate coefficient above 2220 K reported by Mertens et al.[7] is not reproduced by the experimental data of Yokoyama et al.,[58] the more recent data of Romming and Wagner,[59] nor by our own calculations, all of which indicate a decrease in rate coefficient with increasing temperature. From the data in Table 8, we predict that the principal reaction channel is NO + NH → N_2O + H, contributing approximately 90% to the total reaction flux at 2000 K. Reaction to N_2 + OH contributes a further 8% with the balance of about 1% producing O + NNH. When we calculate the rate coefficient for reaction 4 from the rate coefficient for the reverse reaction NO + NH → O + NNH and the equilibrium constant, we retrieve rate coefficients that are in excellent agreement with those obtained by the direct calculations, as listed in Table 7. If, however, we were to assume that the high-temperature data of Mertens et al.[7] essentially correspond to the reaction going completely to O + NNH, we would calculate a rate coefficient of approximately 4×10^{14} cm^3 mol^{-1} s^{-1}, nearly 6 times larger than the Bozzelli and Dean estimate. Such a value would greatly overestimate the NO levels in the modeling studies carried out previously or in the present work.

As mentioned in the Introduction, Hayhurst and Hutchinson[5] reported a value for $k_4K_{P,3}$ from which they then estimated a rate coefficient, k_4, for reaction to NO + NH. Their method involved the assumption that every NH radical produced by reaction 4 rapidly reacts to yield a second NO molecule. For fuel-rich flames of $CH_4/O_2/N_2$ and of $H_2/O_2/N_2$, the above assumption leads to the equation

$$k_4K_{P,3} = \left(\frac{\mathrm{d[NO]}}{\mathrm{d}t}\cdot\frac{1}{2[\mathrm{N_2}][\mathrm{O}]} - k_4\right)\cdot\frac{1}{x_\mathrm{H}} \qquad (17)$$

where x_H is the mole fraction of H in the burnt gas. To obtain x_H, Hayhurst and Hutchinson measured OH and temperature profiles in the burnt gas. There are, however, very significant random errors in their data, ranging from nearly 3 orders of magnitude at 2500 K to nearly 1 order of magnitude at 1800 K. If we fit our computed values of k_4 from the MultiWell simulations and $K_{P,3}$ derived from our thermochemical calculations, we obtain $k_4K_{P,3} = 1.5 \times 10^8 \exp(-3200/T)$ cm^3 mol^{-1} s^{-1}. Comparing with Hayhurst and Hutchinson's value of $k_4K_{P,3} = 1.4 \times 10^9 \exp(-2760/T)$ cm^3 mol^{-1} s^{-1} shows that our value at 2000 K is approximately an order of magnitude lower than theirs, but probably still within the considerable random error in their data.

Kinetic Modeling. As discussed earlier, detailed chemical reaction models, such as the two formulations of GRIMech,[3,4] containing the rate coefficient for k_4 estimated by Bozzelli and Dean[2], have recently been found to overestimate the level of NO produced by combustion systems. We have chosen to use the GRIMech 3.0 model with our new NNH thermochemistry and kinetics. The value of k_4 in this model was altered to the value given in Table 7 and the other three addition and decomposition reaction channels also included together with the direct abstraction of H by O atoms. This modified mechanism has been used to model two series of data[60] from a completely stirred reactor: a fuel lean methane/air combustion and a lean combustion of CO/H_2/air at residence times, τ, between about 3 to 4 ms and equivalence ratios, ϕ, between ~0.5 and 0.6. The first of these cases has been used to benchmark the performance of GRIMech.[4] Figure 5 compares the performance of our modified kinetic model with that of the original GRIMech 3.0 formulation and experimental NO profiles. The modeling was performed using the Chemkin 3.6 AURORA code.[50]

As can be seen from Figure 5(a), both the original formulation of GRIMech 3.0 and our modified version with new NNH thermochemistry and kinetics reproduce the experimental NO data from CH_4/air satisfactorily, although our model gives a

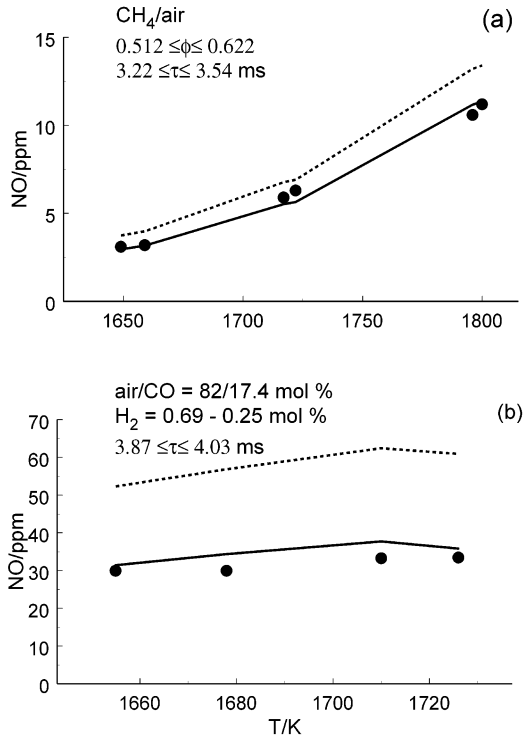

Figure 5. Comparison of NO profiles of combustion in a completely stirred flame reactor. (a) CH_4/air, (b) H_2/CO/air. Filled circles: Experimental data from ref 60. Dashed lines: predictions using GRIMech 3.0. Full lines: prediction using GRIMech 3.0 with NNH thermochemistry and kinetics from the present study.

closer fit to experiment. With the runs in CO/H_2/air (Figure 5(b)), however, significantly poorer performance occurs when using the original GRIMech 3.0 model. Whereas our present model gives a good fit to experiment, GRIMech 3.0 overestimates the level of NO by nearly a factor of 2. To ascertain the reason for this difference in performance, we have carried out reaction path analyses on both kinetic models.

We have sought to quantify the contribution that each of the four reaction pathways makes to NO production by using the following simplified procedure. To determine the contribution of a particular pathway, that pathway is eliminated from the kinetic model and the modified mechanism is then run to ascertain the effect of its omission. This is repeated in turn for each pathway. The basic assumption in this method is that there are no cross correlations between the pathways. It has been shown, however, that the error resulting from neglect of such cross correlation is of 5% or less in the total contribution of all pathways when applied to NO profiles in atmospheric opposed flow methane-air flames.[61] In our present path analysis, the summation error is significantly less than 3%.

The contribution of the thermal pathway is assessed by eliminating its initiation reaction, (1). The prompt-NO pathway contribution was also determined by elimination of its initiation reaction, (2). To assess the contribution of the N_2O intermediate pathway, it was necessary to eliminate all reactions involving N_2O from the reaction model while the NNH + O route was quantified by elimination of its initiation reaction, (4). This procedure is similar to that used previously.[8,61]

Figures 6(a) and (b) compare the contribution of each reaction pathway (viz., Zel'dovich, prompt NO, N_2O, and NNH+O) for our present model and for the original formulation of GRIMech 3.0 to methane-air studies in a completely stirred reactor.[60] The computed contributions of the N_2O intermediate, thermal and prompt-NO pathways are similar for both models. A larger

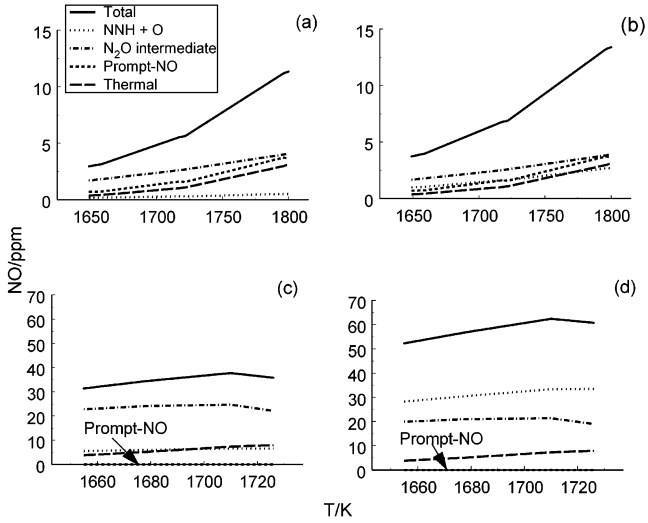

Figure 6. Predictions of the contribution of individual pathways to NO formation. (a) Present model predictions for the CH_4/air data of Figure 5 (a). (b) GRIMECH 3.0 predictions for the CH_4/air data of Figure 5 (a). (c) Present model predictions for the H_2/CO/air data of Figure 5 (b). (d) GRIMECH 3.0 predictions for the H_2/CO/air data of Figure 5 (b).

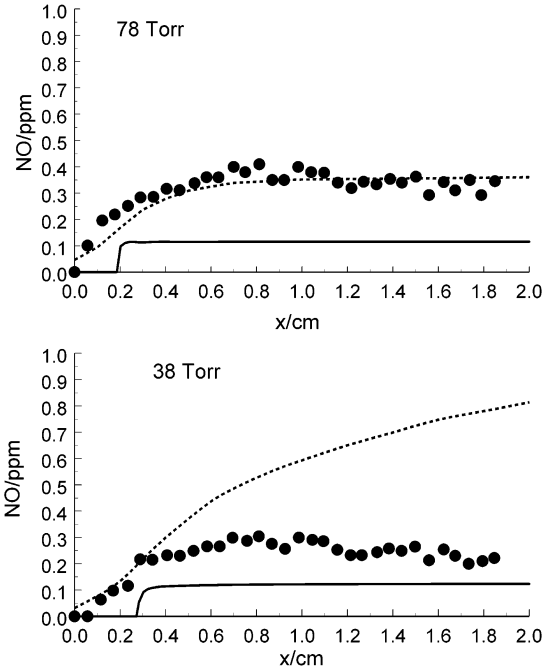

Figure 7. Comparison of experimental LIF NO profiles[6] with predictions using GRIMech 2.11 and our kinetic model for low-pressure H_2/air flames. Filled circles = experimental data, dashed lines = predictions using GRIMech 2.11 and $k_4 = 7 \times 10^{13}$ cm^3 mol^{-1} s^{-1}, full lines = predictions using ab initio thermochemistry and kinetics of this work with GRIMech 3.0.

contribution of the NNH + O pathway is calculated using GRIMech 3.0. Nevertheless, because the first three pathways all make significant contributions to the NO profile, the two models both give reasonable reproductions of the experimental data, although GRMech 3.0 does somewhat overestimate the NO levels. It is with the runs in CO/H_2/air (Figure 6 (c) and (d)), however, that the computed contributions of the two models radically differ. The prompt-NO pathway makes no contribution in these runs. Again, the calculated contributions of the N_2O and thermal pathways are quite similar for both models; however, GRIMech 3.0 predicts that the NNH + O pathway

will make the greatest contribution to the NO profiles, whereas our model, with new NNH thermochemistry and kinetics, predicts that this pathway makes only a very small contribution to the total. It is apparent, therefore, that by overestimating the contribution of the NNH + O pathway GRIMech 3.0 predicts too high a level of NO in this system. In methane-air combustion where there are significant contributions from the prompt and thermal routes, the overestimation of the NNH + O pathway is masked. Where the prompt and thermal pathways are minimized, this overestimation becomes obvious.

At the suggestion of a reviewer, we have also used our new thermochemistry and kinetics to attempt to model the low-pressure premixed H_2/air flames studied by Harrington et al.[6] The modeling was carried out using the Chemkin 3.6 PREMIX code. Harrington et al. originally employed the GRIMech 2.11 mechanism[3] to model their laser induced fluorescence NO profiles and we compare the predictions of our model with their experimental and modeled data in Figure 7. At both 78 and 38 Torr, our model underpredicts the experimental NO profiles. However, while the GRIMech 2.11 formulation gives a good prediction of NO at 78 Torr, it significantly overpredicts the NO profile at 38 Torr. Incidentally, the Bozzelli and Dean rate coefficient[2] for k_4 when used with the GRIMech 3.0 thermochemistry for NNH leads to slightly higher model profiles than those obtained by Harrington et al.[6] with GRIMech 2.11. An increase in the A-factor of our rate coefficient by a factor of 2 for reaction 4 leads to good agreement with experiment at 38 Torr and only to a slight underprediction at 78 Torr. Of course, an increase by a factor of 2 would then lead to an overprediction of the profiles presented in Figure 5 for the completely stirred reactor.

A detailed testing of our new thermochemistry and kinetics in modeling atmospheric premixed and opposed flow flames will be presented elsewhere.[62]

Conclusions

Three reaction potential energy surfaces for NNH + O → products have been investigated by ab initio quantum chemical calculations. Three adducts, namely, *trans*-ONNH, *cis*-ONNH and ONHN, have been identified, through which reaction to three exothermic product channels, NO + NH, N_2 + OH, N_2O + H, and one endothermic channel, HNO + N, take place. Rate coefficients to each reaction channel have been obtained by RRKM analysis. The rate coefficient at 2000 K to the NO + NH channel is predicted to be approximately a factor of 4 lower than had been previously estimated[2] (and included in detailed reaction models such as GRIMech 3.0[4]). A new value of $\Delta_f H^\circ_{298}$ (NNH) = 60.6 ± 0.5 kcal mol^{-1} has been obtained by CCSD(T) calculations, which include extrapolation to the complete basis limit. This value, together with the rate coefficients we have derived for the NNH + O → products reactions, have been used to modify the GRIMech 3.0 reaction model. Using this new formulation, we could satisfactorily model NO profiles produced in a completely stirred reactor[60] from both methane-air and CO/H_2/air mixtures. Overestimation of NO profiles from the latter mixtures by GRIMech 3.0 has been shown, by reaction path analysis, to result from too high a rate coefficient for initiation of the NNH + O pathway. On the basis of the present work, we conclude that this pathway represents a very minor route to NO in most combustion systems.

Acknowledgment. We wish to express our thanks to the Australian Partnership for Advanced Computing National Facility for access to the COMPAQ AlphaServer SC system. N. L. H. gratefully acknowledges the receipt of an Australian Postgraduate Research Scholarship.

Supporting Information Available: Corresponding geometries, rotational constants, and vibrational frequencies. This material is available free of charge via the Internet at http://pubs.acs.org.

References and Notes

(1) Miller, J. A.; Bowman, C. T. *Prog. Energy Combust. Sci.* **1989**, *15*, 287.
(2) Bozzelli, J. W.; Dean, A. M. *Int. J. Chem. Kinet.* **1995**, *27*, 1097.
(3) Bowman, C. T.; Hanson, R. K.; Davidson, D. F.; Gardiner, W. P., Jr; Lissianski, V.; Smith, G. P.; Golden, D. M.; Frenklach, M.; Goldenberg, M. GRIMech; 2.11 ed.
(4) Smith, G. P.; Golden, D. M.; Frenklach, M.; Moriaty, N. W.; Eiteneer, B.; Goldenberg, M.; Bowman, C. T.; Hanson, R. K.; Song, S.; Gardiner, W. C. J.; Lissianski, V. V.; Qin, Z. GRIMech; 3.0 ed.
(5) Hayhurst, A. N.; Hutchinson, E. M. *Combust. Flame* **1998**, *114*, 274.
(6) Harrington, J. E.; Smith, G. P.; Berg, P. A.; Noble, A. R.; Jeffries, J. B.; Crosley, D. R. In *Twenty-Sixth Symp.* (*Int.*) *on Combustion*; The Combustion Institute: Pittsburgh, PA, 1996; p 2133.
(7) Mertens, J. D.; Chang, A. Y.; Hanson, R. K.; Bowman, C. T. *Int. J. Chem. Kinet.* **1991**, *13*, 173.
(8) Charlston-Goch, D.; Chadwick, B. L.; Morrison, R. J. S.; Campisi, A.; Thomsen, D. D.; Laurendeau, N. M. *Combust. Flame* **2001**, *125*, 729.
(9) Konnov, A. A.; De Ruyck, J. *Combust. Flame* **2001**, *125*, 1258.
(10) Melius, C. F.; Binkley, J. S. In *Twentieth Symp.* (*Int.*) *on Combustion*; The Combustion Institute: Pittsburgh, PA, 1984; p 575.
(11) Marshall, P.; Fontijn, A.; Melius, C. F. *J. Chem. Phys.* **1987**, *86*, 5540.
(12) Fueno, T.; Fukuda, M.; Yokoyama, K. *Chem. Phys.* **1988**, *124*, 265.
(13) Harrison, J. A.; MacIagan, R. G. A. R. *J. Chem. Soc., Faraday Trans.* **1990**, *86*, 3519.
(14) Walch, S. P. *J. Chem. Phys.* **1993**, *98*, 1170.
(15) Durant, J. L., Jr. *J. Phys. Chem.* **1994**, *98*, 518.
(16) Bradley, K. S.; McCabe, P.; Schatz, G. C.; Walch, S. P. *J. Chem. Phys.* **1995**, *102*, 6696.
(17) Simonson, M.; Bradley, K. S.; Schatz, G. C. *Chem. Phys. Lett.* **1995**, *244*, 19.
(18) Kristyan, S.; Lin, M. C. *Chem. Phys. Lett.* **1998**, *297*, 200.
(19) van Beek, M. C.; ter Meulen, J. J. *J. Chem. Phys.* **2001**, *115*, 1843.
(20) Walch, S. P.; Partridge, H. *Chem. Phys. Lett.* **1995**, *233*, 331.
(21) Gu, J.; Xie, Y.; Schaefer, H. F., III. *J. Chem. Phys.* **1998**, *108*, 8029.
(22) Curtiss, L. A.; Redfern, P. C.; Raghavachari, K.; Pople, J. A. *J. Chem. Phys.* **2001**, *114*, 108.
(23) Hampel, C.; Peterson, K. A.; Werner, H.-J. *Chem. Phys. Lett.* **1992**, *190*, 1.
(24) Raghavachari, K.; Trucks, G. W.; Pople, J. A.; Head-Gordon, M. *Chem. Phys. Lett.* **1989**, *157*, 479.
(25) Dunning, T. H., Jr. *J. Chem. Phys.* **1989**, *90*, 1007.
(26) Kendall, R. A.; Dunning, T. H., Jr.; Harrison, R. J. *J. Chem. Phys.* **1992**, *96*, 6796.
(27) Woon, D. E.; Dunning, T. H., Jr. *J. Chem. Phys.* **1993**, *98*, 1358.
(28) Becke, A. D. *J. Chem. Phys.* **1993**, *98*, 5648.
(29) Becke, A. D. *Phys. Rev. A* **1988**, *38*, 3098.
(30) Lee, C.; Yang, W.; Parr, R. G. *Phys. Rev. B* **1988**, *37*, 785.
(31) Helgaker, T.; Klopper, W.; Koch, H.; Noga, J. *J. Chem. Phys.* **1997**, *106*, 9639.
(32) Cowan, R. D.; Griffin, D. C. *J. Opt. Soc. Am.* **1976**, *66*, 1010.
(33) Martin, R. L. *J. Phys. Chem.* **1983**, *87*, 750.
(34) Roos, B. O.; Taylor, P. R.; Siegbahn, P. E. M. *Chem. Phys.* **1980**, *48*, 157.
(35) Roos, B. O. In *Ab Initio Methods in Quantum Chemistry II*; Lawley, K. P., Ed.; J. Wiley & Sons Ltd.: Chichester, UK, 1987; Vol. LXIX.; p 399.
(36) Curtiss, L. A.; Raghavachari, K.; Redfern, P. C.; Rassolov, V.; Pople, J. A. *J. Chem. Phys.* **1998**, *109*, 7764.
(37) Pollack, E. In *Theory of Chemical Reaction Dynamics*; Baer, M., Ed.; CRC Press: Boca Raton, FL, 1985; Vol. 3; p 128.
(38) Hase, W. L.; Mondro, S. L.; Duchovic, R. J.; Hirst, D. M. *J. Am. Chem. Soc.* **1987**, *109*, 2916.
(39) Truhlar, D. G.; Garrett, B. C. *Acc. Chem. Res.* **1980**, *13*, 440.
(40) Mackie, J. C.; Bacskay, G. B.; Haworth, N. L. *J. Phys. Chem. A* **2002**, *106*, 10825.
(41) Steinfeld, J. I.; Francisco, J. S.; Hase, W. L. *Chemical Kinetics and Dynamics*; Prentice Hall: Engelwood Cliffs, NJ, 1989.

(42) Shavitt, I. *J. Chem. Phys.* **1959**, *31*, 1359.

(43) Frisch, M. J.; Trucks, G. W.; Schlegel, H. B.; Scuseria, G. E.; Robb, M. A.; Cheeseman, J. R.; Zakrzewski, V. G.; Montgomery, J. A., Jr.; Stratmann, R. E.; Burant, J. C.; Dapprich, S.; Millam, J. M.; Daniels, A. D.; Kudin, K. N.; Strain, M. C.; Farkas, O.; Tomasi, J.; Barone, V.; Cossi, M.; Cammi, R.; Mennucci, B.; Pomelli, C.; Adamo, C.; Clifford, S.; Ochterski, J.; Petersson, G. A.; Ayala, P. Y.; Cui, Q.; Morokuma, K.; Malick, D. K.; Rabuck, A. D.; Raghavachari, K.; Foresman, J. B.; Cioslowski, J.; Ortiz, J. V.; Stefanov, B. B.; Liu, G.; Liashenko, A.; Piskorz, P.; Komaromi, I.; Gomperts, R.; Martin, R. L.; Fox, D. J.; Keith, T.; Al-Laham, M. A.; Peng, C. Y.; Nanayakkara, A.; Gonzalez, C.; Challacombe, M.; Gill, P. M. W.; Johnson, B. G.; Chen, W.; Wong, M. W.; Andres, J. L.; Head-Gordon, M.; Replogle, E. S.; Pople, J. A. *Gaussian 98*, revision A.7; Gaussian, Inc.: Pittsburgh, PA, 1998.

(44) Knowles, P. J.; Hampel, C.; Werner, H.-J. *J. Chem. Phys.* **1993**, *99*, 5219.

(45) Amos, R. D.; Bernhardsson, A.; Berning, A.; Celani, P.; Cooper, D. L.; Deegan, M. J. O.; Dobbyn, A. J.; Eckert, F.; Hampel, C.; Hetzer, G.; Knowles, P. J.; Korona, T.; Lindh, R.; Lloyd, A. W.; McNicholas, S. J.; Manby, F. R.; Meyer, W.; Mura, M. E.; Nicklass, A.; Palmieri, P.; Pitzer, R.; Rauhut, G.; Schütz, M.; Schumann, U.; Stoll, H.; Stone, A. J.; Tarroni, R.; Thorsteinsson, T.; Werner, H.-J..MOLPRO: a package of ab initio programs designed by H.-J. Werner and P. J. Knowles; version 2002.6.

(46) Helgaker, T.; Jensen, H. J. A.; Jørgensen, P.; Olsen, J.; Ruud, K.; Aagren, H.; Andersen, T.; Bak, K. L.; Bakken, V.; Christiansen, O.; Dahle, P.; Dalskov, E. K.; Enevoldsen, T.; Fernandez, B.; Heiberg, H.; Hettema, H.; Jonsson, D.; Kirpekar, S.; Kobayashi, R.; Koch, H.; Mikkelsen, K. V.; Norman, P.; Packer, M. J.; Saue, T.; Taylor, P. R.; Vahtras, O. DALTON; Release 1.0, **1997**.

(47) Andersson, K.; Blomberg, M. R. A.; Fülscher, M. P.; Karlström, G.; Lindh, R.; Malmqvist, P.-Å.; Neogrády, P.; Olsen, J.; Roos, B. O.; Sadlej, A. J.; Schültz, M.; Seijo, L.; Serrano-Andrés, L.; Siegbahn, P. E. M.; Widmark, P.-O. MOLCAS; Version 4; Lund University: Lund, Sweden, **1997**.

(48) Barker, J. R. Multiwell Software; Version 1.2.0 Ann Arbor, MI, **2002**.

(49) Barker, J. R. *Int. J. Chem. Kinet.* **2001**, *33*, 232.

(50) Kee, R. J.; Rupley, F. M.; Miller, J. A.; Coltrin, M. E.; Grcar, J. F.; Meeks, E.; Moffat, H. K.; Lutz., A. E.; Dixon-Lewis, G.; Smooke, M. D.; Warnatz, J.; Evans, G. H.; Larson, R. S.; Mitchell, R. E.; Petzold, L. R.; Reynolds, W. C.; Caracotsios, M.; Stewart, W. E.; Glarborg, P.; Wang, C.; Adigun, O. CHEMKIN Collection; Release 3.6; Reaction Design, Inc.: San Diego, CA, **2000**.

(51) Tarroni, R.; Palmieri, P.; Mitrushenkov, A.; Tosi, P.; Barsi, D. *J. Chem. Phys.* **1997**, *106*, 10265.

(52) Chase, M. W., Jr. *J. Phys. Chem. Ref. Data* **1998**, *Monograph 9*, 1.

(53) Rusic, B.; Feller, D.; Dixon, D. A.; Peterson, K. A.; Harding, L. B.; Asher, R. L.; Wagner, A. F. *J. Phys. Chem. A* **2001**, *105*, 1.

(54) Anderson, W. R. *Combust. Flame* **1999**, *117*, 394.

(55) Wilson, A. K.; van Mourik, T.; Dunning, T. H., Jr. *J. Mol. Struct.* (*THEOCHEM*) **1996**, *388*, 339.

(56) van Mourik, T.; Wilson, A. K.; Dunning, T. H., Jr. *Mol. Phys.* **1999**, *96*, 529.

(57) Lillich, H.; Schuck, A.; Volpp, H.-R.; Wolfrum, J. In *Twenty-Fifth Symp.* (*Int.*) *on Combustion*; The Combustion Institute: Pittsburgh, PA, 1994; p 993.

(58) Yokoyama, K.; Sakane, Y.; Fueno, T. *Bull. Chem. Soc. Jpn.* **1991**, *64*, 1738.

(59) Romming, H. T.; Wagner, H. G. In *Twenty-Sixth Symp.* (*Int.*) *on Combustion*; The Combustion Institute: Pittsburgh, PA, 1996; p 559.

(60) Steele, R. C.; Malte, P. C.; Nicol, D. G.; Kramlich, J. C. *Combust. Flame* **1995**, *100*, 440.

(61) Thomsen, D. D.; Laurendeau, N. M. *Combust. Flame* **2001**, *124*, 350.

(62) Mackie, J. C.; Haworth, N. L.; Bacskay, G. B., Submitted to Australian Symposium on Combustion, Melbourne, December, 8−9, 2003.